Review: Ultraviolet Fluorescence as Assessment Tool for Photovoltaic Modules

Marc Köntges, Arnaud Morlier, Gabriele Eder, Eckhard Fleiß, Bernhard Kubicek, and Jay Lin

***Abstract*—Since 2010, the ultraviolet fluorescence (UVF) method is used to identify defects in wafer-based crystalline silicon photovoltaic (PV) modules. We summarize all known applications of fluorescence imaging methods on PV modules to identify defects and characteristics. The aim of this review is to present the basic principles for the interpretation of UVF images. The method allows for detection of cell cracks in a chronological order of occurrence, visualizing hot parts in a PV module, and identifying deviating bill of materials of PV modules. The effects of various material combinations on the UVF are reproduced in the lab and explained for the first time. Seasonal effects on the UVF are presented for the first time. In addition, some not yet understood features in the images are shown and discussed. Furthermore, the application of UVF imaging for manual, hood-based, and drone-based inspection is presented. The analysis speed of the three methods has been measured under real conditions. For the manual inspection, we found an evaluation speed of 250 modules/h, for a hood-based system 200 modules/h and the drone-based method allows an imaging speed of up to 720 modules/h.**

***Index Terms*—Ultraviolet fluorescence, power system reliability, solar panels, fault diagnosis.**

I. Introduction

ULTRAVIOLET fluorescence (UVF) measurements are widely used for many applications. In biology, the method is used to track gene activation or to follow specific reaction paths in organic cells [1]. Analytical tools exist to scan for fluorescent markers in a living animal [2]. For the analysis of paintings even spectrally resolved imaging is used to identify materials in the artwork [3]. The police uses the UVF method to identify otherwise invisible traces at a crime scene [4]. For photovoltaic (PV) application, Pern reported in 1996 for the first time the application of UVF to analyze the degradation of the encapsulant (yellowing effect) in PV modules [5]. In 2000, King showed an UVF image of an entire PV module for the first time [6]. In 2010, Schlothauer proved that dark lines in the UVF images of PV modules correlate with cracks in the solar cells [7], [8]. One of the authors demonstrated the application of the method in a PV system to analyze the fraction of cell cracks in PV modules [9]. Multiple publications followed describing the development of mobile measurements systems, enabling PV applications of UVF imaging and spectroscopy both in the field and the laboratory [10], [11], [12], [13], [14].

In the following chapters, we introduce the basics of the UVF method as it is used for PV module inspection. The origin of UVF generation and photobleaching is explained for various typical PV-related examples [12], [15], [16]. Subsequently, various factors influencing the formation of UVF in polymeric PV materials are presented and their impact on the quantity of fluorescent species (=fluorophores), which determines the intensity of the measurable UVF of PV modules, is discussed. Furthermore, we give a detailed look on the applicability of the method for PV module reliability analysis and on the practicability of the method.

II. Description of the UV Fluorescence Methods

The UVF method relies on fluorescence effects of the polymeric lamination material in a PV module. This is typically Ethylene vinyl acetate (EVA) added with various additives such as oxidation stabilizers, UV absorbers, and the crosslinker [17]. Fluorescence is a form of luminescence, which is the emission of light by an activated material that has absorbed light or other electromagnetic radiation. The reemitted light (e.g., in the visible region) has a longer wavelength than the absorbed radiation (e.g., UV light). A fluorophore is thus a fluorescent chemical compound that can reemit light upon light excitation and mostly contains several combined aromatic groups or other plane or cyclic molecule groups with several π bonds. Typical fluorophores are degradation products of polymers and/or additives with chromophore/fluorophore groups. The fluorescence of materials can be extinguished by "photobleaching" effects which lead to a decrease of fluorescence because of reaction processes with, e.g., oxygen [5], [18], [19], [20].

UVF can be performed spatially resolved using a spectrometer and a UV irradiation source. The resulting spectrum contains contributions of both, the spectral UVF response of the investigated materials, and the reflectance residue of the light source.

Manuscript received November 18, 2019; revised December 14, 2019; accepted December 19, 2019. Date of publication January 14, 2020; date of current version February 19, 2020. This work was supported in part by the German Federal Ministry for Economic Affairs and Energy under Grant 0325735D and Grant 0324304C, and in part by the Austrian Klima- & Energiefonds under the project "AMSEL," FFGnr.:848771. *(Corresponding author: Marc Köntges.)*

M. Köntges and A. Morlier are with the Institute for Solar Energy Reasearch Hamelin, 31860 Emmerthal, Germany (e-mail: m.koentges@isfh.de; a.morlier@isfh.de).

G. Eder is with the Austrian Research Institute for Chemistry and Technology, 1030 Vienna, Austria (e-mail: gabriele.eder@ofi.at).

E. Fleiß is with the Fleiss Engineering, 31832 Springe-Eldagsen, Germany (e-mail: mail@fleiss.info).

B. Kubicek is with the Austrian Institute of Technology GmbH, 1210 Vienna, Austria (e-mail: bernhard.kubicek@ait.ac.at).

J. Lin is with the PV Guider Consultancy, Taipei 114, Taiwan (e-mail: jay@pvguider.com).

Color versions of one or more of the figures in this article are available online at http://ieeexplore.ieee.org.

Digital Object Identifier 10.1109/JPHOTOV.2019.2961781

To minimize potential overlays, either a monochromatic source (e.g., a laser) or a bandwidth limited light emitting diode (LED) with an emission spectrum outside the observed spectral range can be used for excitation. Schlothauer mounted an assembly of a spectrometer and laser excitation source onto a one- or two-dimensional scanning setup to record spectral resolved images of whole PV modules [21], [22].

However, a simpler method is to irradiate the whole PV module with an excitation light source, and observe the fluorescence effect either with the naked eye or with a photo camera (UVF imaging). Both detection options operate in three spectral ranges (red, green, and blue), according to the physiology of the human eye that the camera emulates. Hence, some qualitative spectral information is also contained in the imaging methods. Because of the small efficiency of the UVF conversion and limited emission power of UV LEDs, imaging is often performed in dark environments.

The excitation of PV modules with UV light is commonly achieved using LEDs in the spectral range from 350 nm (glass transmission) to 380 nm (human visibility border). An additional short pass filter can be used to cut off residual visible light of the light source thus creating better contrast. For further image improvement, a long pass filter in front of the camera can be used to exclude the excitation light from the image.

In general, UVF measurements are nondestructive, noninvasive, easy to handle, and fast [9], [11], [23]. The UVF images presented in this article are acquired by experimental UVF imaging setups with or without filters.

III. Origins of UVF in PV Modules

Typical PV modules are composed of a front glass sheet, a polymeric lamination material embedding the silicon wafer-based solar cells, cell interconnect ribbons, and a protective polymeric backsheet. In this article, we focus on this type of module design.

Some of these components contain substances with the ability to fluoresce or which develop fluorescing degradation products during their lifetime. In principle, only materials that are capable of absorbing UV photons can produce a UVF effect.

A. UVF of the Front Glass of a PV Module

Front glasses of PV modules are typically transparent in the UVA range (315–400 nm) [24]. Thus, an excitation of the polymeric lamination material with UVA light is possible. Even glasses can fluoresce under UV light because of the presents of color centers in the glass matrix [25], [26] or tin oxide (refining agent) which is created during the production of floating glass. The melt of float glass is floated on a tin bath to create a perfect flat glass plate. To excite the tin oxide of the float glass, a UV source of typically 254 nm is used to determine the floating side of a glass plate. To protect the laminate against UV-radiation former, PV modules used cerium-containing glasses. Cerium shifts the UV cut off of 3-mm thick glass up to 350 nm [27]. Therefore, UVF can be excited in this glass type with excitation light of up to 350 nm. Cerium is no longer used in current glasses for PV modules. To avoid interfering UVF effects or absorption in the front glass of a PV module, the excitation spectrum should have no spectral parts below 315 nm.

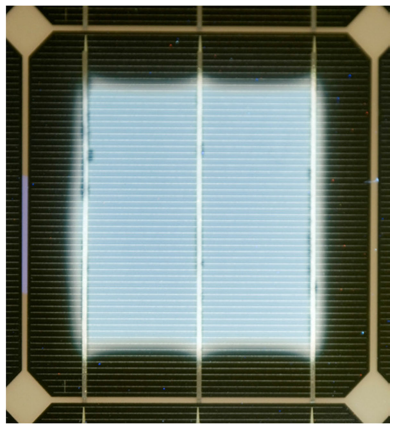

Fig. 1. Build-up of UVF in the core of the encapsulation material between the front glass and cell; photobleaching takes place along the edge of the cell.

B. UVF of the Lamination Material After Manufacturing

The UVF intensity emitted by the encapsulant EVA increases with lamination time at typical module lamination temperatures (150–160 °C). This UVF intensity is correlated to the degree of crosslinking of the material and originates from fluorescent by-products between crosslinking activators and other additives in the material [15], [28], [29]. This opens the potential for using in-line UVF measuring devices to assess the curing state of crosslinked encapsulation material within a PV module. These fluorophores are nevertheless rapidly extinguished during the first days under sun exposure [10].

C. UVF of the Encapsulation in front of a Solar Cell

In front of the solar cell, UV radiation and high temperatures can form fluorescent groups. Because of the Lambert–Beer absorption distribution for the UV radiation in the encapsulant, the concentration of the fluorescent products is exponentially distributed between the front glass and the solar cell. The concentration is highest on the front glass and lowest on top of the solar cell of the PV module [30]. The front glass and the silicon solar cell beneath the lamination material are an effective barrier for these degradation products. These diffusion barriers lead to an accumulation of degradation products in the front encapsulant and give rise to a lateral uniform UVF. With increasing time, molecules from the rear (rear lamination material, backsheet, and primarily oxygen and/or water vapor from the ambient air) can diffuse into the front encapsulant starting from the cell gaps. The diffusion path all around the solar cell is typically very long (multiple cm), thus it takes time for the oxygen to reach the front encapsulant. Fig. 1 shows the UVF distribution in front of a field aged encapsulated defect free solar cell of a glass/backsheet module being exposed in central European climate for three years.

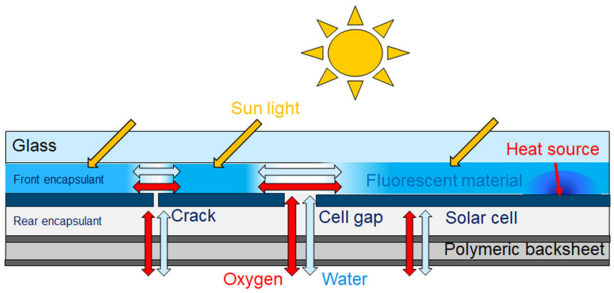

Fig. 2. Schematic representation of the cross-sectional view of a PV module illustrating the permeation paths within a PV module stack. The UV spectrum of the sunlight generates fluorescent material in the front encapsulant; oxygen in the presence of irradiation bleaches the UVF in the gap between the cells and above cell cracks resulting in a specific UVF pattern.

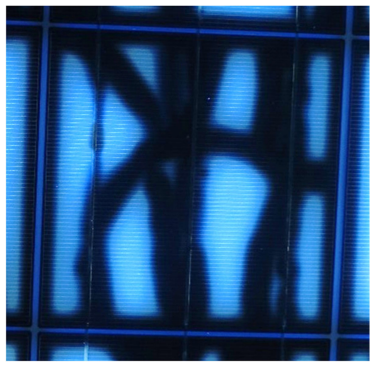

Fig. 3. Photobleaching of the UVF along the edge and cracks of the solar cell. The glass/backsheet module was weathered in central Italy for two years.

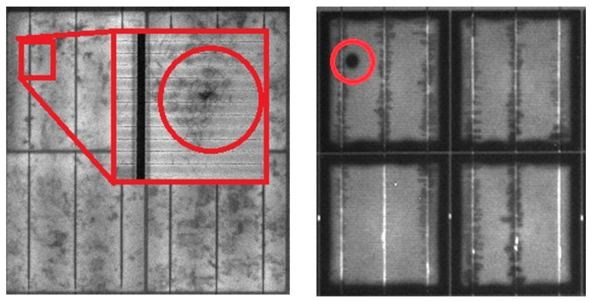

Fig. 4. Left: EL image of a solar cell in a PV module with an inset of a 1–2 mm long cross crack. Right: UVF image of the same cell with a black spot at the cross crack position. The modules were exposed in south Germany for two years.

D. UVF of the Encapsulant Between Solar Cells

In between the cells, the diffusion path to and from the ambient air is maximum 1 mm for typical backsheet type modules. Therefore, the chemical ambient between the cells is clearly different from that in front of the cell, see Fig. 2. As the oxygen molecules can interact (e.g., energy transfer, collision, and reaction) with the activated and fluorescing sites of the polymer, its presence leads to a decrease of the UVF intensity. Bleaching needs irradiation besides oxygen (photobleaching) [16].

E. UVF in the Encapsulant Along the Edges of the Solar Cells

Along the edge of the solar cells, there is a region where molecules can diffuse from the cell gap into the front encapsulant above the cell. In this edge region, we can follow the competition between UVF generation and photobleaching processes. With increasing operational time of the PV module and pronounced ingress of oxygen, this effect causes a photobleached (darkend) rim along the cell edge (square pattern). However, if there are different encapsulation materials used for front and rear encapsulation, material exchange because of concentration differences will also take place. In this area (edges and interspaces between the cells), we thus achieve an intermixture of permeating molecules from the front and rear encapsulation materials of the PV module and environmental molecules like water vapor and oxygen. This special situation may lead to unexpected UVF patterns in aged PV modules along the cell edge which are explained in a later chapter.

F. UVF in the Encapsulant Above Cell Cracks

Above cell cracks, similar UVF photobleaching effects can happen as at the edge of the solar cell. Oxygen penetrates the cell through the cell crack and, in combination with sunlight, the UVF above the crack is photobleached, see Fig. 3. In case that the cell cracks were introduced before the installation of the PV module took place, the photobleaching pattern above a cell crack is about double as wide as the photobleaching pattern along the cell edge. The oxygen spreads to the right and left of a cell crack, whereas the oxygen along the cell edge can only diffuse toward the center of the cell.

In the previous article, it was investigated which fraction of solar cell cracks detectable with electroluminescence (EL) imaging are also traceable with UVF [31]. Twenty fielded PV modules with cell cracks were characterized with UVF in the lab. It could be proven that all cracks seen in the EL image were also visible in the UVF image. Thus, it was concluded that cell cracks are almost always an open diffusion pass for molecules from the rear to the front of the cell as it is between the cells. However, between the cells also light can pass through the cells and interact with the inner backsheet surface, which is not the case for the cell crack area. For light sensitive backsheets which form fluorophores upon irradiation, different effects might occur for cell cracks and cell gaps within the same PV module, e.g., Fig. 3.

Cell cracks may show a grey brownish or black discoloration along the crack on top of the silver finger of the solar cells. These discolorations are called “snail tracks” and exists in at least four different types of appearance and root cause mechanisms [32], [33], [34]. UVF images of snail track affected modules show the typical black structure in the area above the cell cracks. However, to the best of our knowledge, snail track affected modules do not show additional UVF features compared with modules with only cell cracks.

G. UVF Along the Cell Interconnect Ribbon

The flux used for the interconnection process of the solar cells and the cell interconnect ribbon can be a source of fluorophores

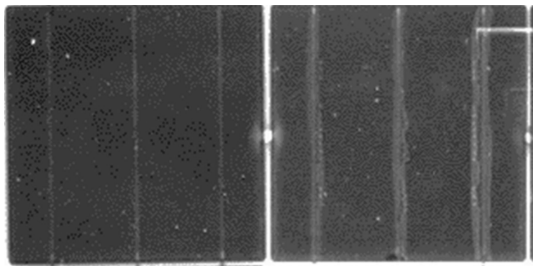

Fig. 5. Part of a laminate artificially exposed to UV (72 kWh/m²) with the bus bars of the right cell have been fluxed with surplus of flux. The spot between the cells originates from a string fixing tape.

[35], [36]. The flux mainly consists of the solvent isopropyl alcohol. The main functional ingredient is colophony containing slightly oxidizing resin acids such as abietin and pimaric acid. In practice, only fluxes with a very high content of colophony show detectable UVF effects either on the cell interconnect ribbon or on the cell in the case of accidentally surplus flux application on top of the cell. This leads to a broad UVF near the bus bars. Fig. 5 shows a PV mini module in which the right cell has been soldered with a surplus of a halogen-free and nonrosin flux from Kester. The mini module was stored under a UV lamp for a total dose of ca. 72 kWh/m². A fluorescent trail appears along the flux remains and the UVF intensity increases with increasing dispensed amount of flux.

The solar cell reflects almost 0% of the excitation and fluorescence signal. On the contrary, typical cell interconnector ribbons have a reflectance of approx. 70% in the visible spectrum. Therefore, the UV radiation is reflected at the cell interconnect ribbon. This is the reason for the formation of more fluorescent degradation products above the ribbon compared with the pure cell area. Furthermore, during the measurement, the exciting UV irradiation and the excited fluorescence radiation is also reflected at the cell interconnect ribbon. These three effects result in a significant increased fluorescence signal compared with the fluorescence above the cell, even if no flux is applied Therefore, only increased fluorescence trails besides but along the cell interconnect ribbon are an unambiguous sign for a surplus of flux.

H. Effect of Lamination Material Type and Material Combinations on UVF Patterns

Different qualities/types of encapsulant can also cause varying UVF effects as not only the polymer itself but also impurities, cross linker decomposition products and additives (and their degradation products) can show fluorescence [37]. So far, the UVF technique has been successfully applied to modules encapsulated with thermoplastic silicones, cross linking polyolefins (PO) [38] as well as with various EVA types [7], [10], [23]. Materials with short cut off wavelength in the UVA domain tend to develop less fluorophores than their UVA absorbing peers.

Fig. 6 shows UVF images of four one-cell modules with different combinations of encapsulants and backsheets after artificial UV loading.

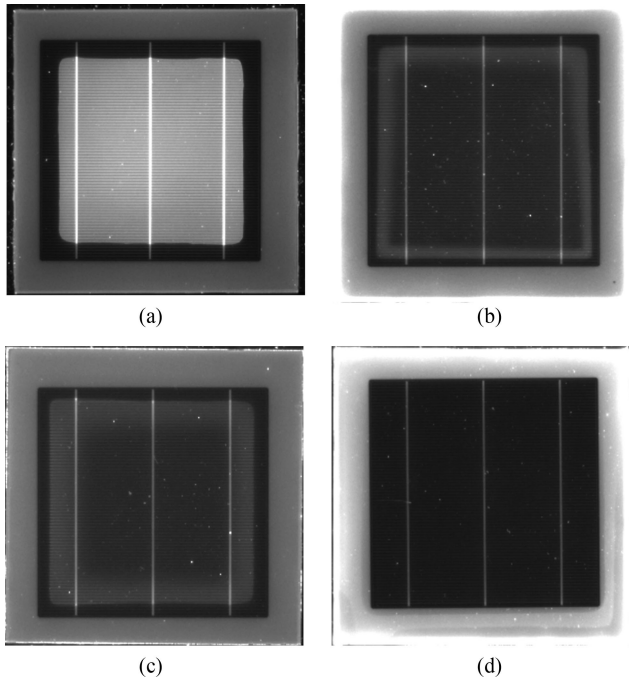

Fig. 6. UVF of one-cell laminates with different materials after exposure to 172 kWh/m² UV light. The respective material combinations are given above each image. (a) Front: UVA abs. EVA Rear: UVA abs. EVA Backsheet 1. (b) Front: UVA trans. PO Rear: UVA abs. PO Backsheet 2. (c) Front: UVA trans. PO Rear: UVA abs. PO Backsheet 1. (d) Front: UVA trans. PO Rear: UVA trans. PO Backsheet 2.

One of the modules is laminated with an UVA absorbing EVA. The other three modules are encapsulated with PO: one comprises of UVA transparent PO, the other modules are made with a combination of UVA-absorbing (rear encapsulant) and UVA transparent (front encapsulant) PO. The EVA module shows the known square pattern of UVF with a dark frame along the cell edges [Fig. 6(a)]. The module encapsulated with UVA transparent PO does not show any UVF pattern above the cell. Nevertheless, above the backsheet around the cell UVF was observed. This shows the importance of UV absorbers in the encapsulant material to protect the backsheet from alteration through UV exposure.

The two modules with the different PO show a UVF ring inside the usual dark frame at the cell edges [Fig. 6(b) and (c)]. This ring is intensely fluorescing at the frontier with the dark frame and the intensity decreases toward the center of the cell. As it was shown that the UVA transparent material does not lead to the enhanced formation of fluorophores under UV exposure in this experiment [Fig. 6(d)], the observed pattern suggests that the UV absorber from the back encapsulant diffuses into the front encapsulant and leads to an inhomogeneous distribution of UV absorber over the cell.

The proposed mechanism for the formation of the ring pattern is illustrated in Fig. 7. The shown module uses UVA transparent EVA on the front side and UVA absorbing EVA on the rear side. Along the cell gaps the UVA absorber molecules from the rear encapsulant diffused into the front of the cell rim area and formed fluorophores upon irradiation. The main fraction of the

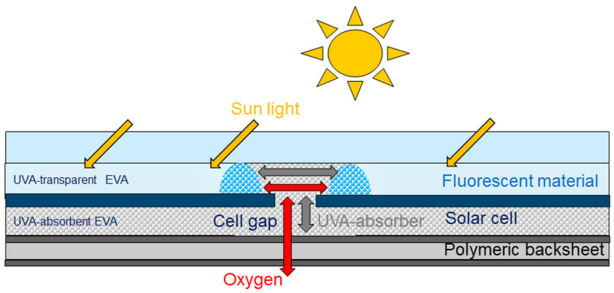

Fig. 7. Fluorescence effect for UVA-transparent EVA on the front and UVA absorbing EVA on the rear. UVA absorber diffuses during the lamination process from the rear EVA to the front of the cells near the cell gap.

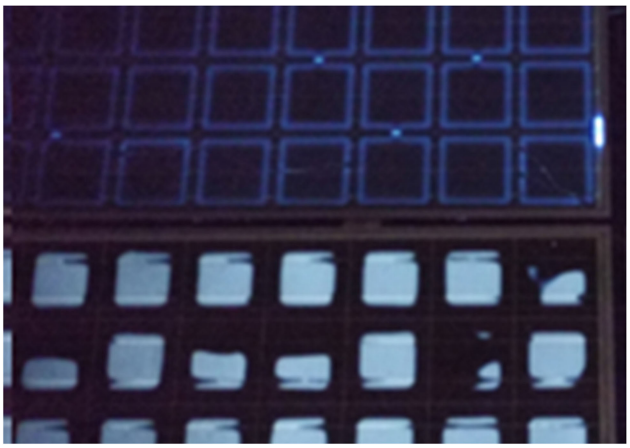

Fig. 8. Ring (one-year old) and square (four years) UVF-pattern of two glass/backsheet modules exposed in Taiwan.

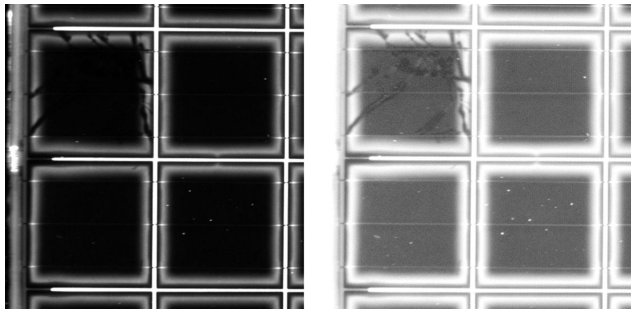

Fig. 9. Left: UVF image (ring pattern) of a PV module with fluorescent backsheet in the cell gaps. Right: Left image in logarithmic scale. The photobleached UVF of one cracked cell can be identified.

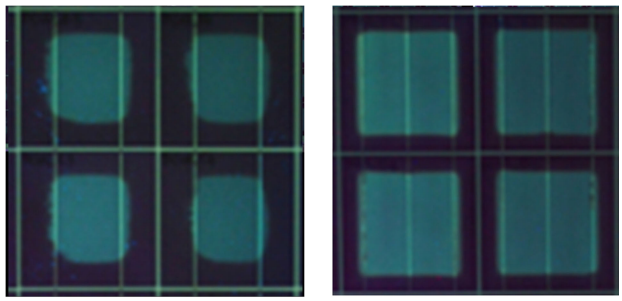

Fig. 10. Fluorescence pattern of naturally aged (~5 years) modules with identical service life and site of installation but two backsheet types: left: Polyamid with high OTR, right: Tedlar with low OTR [16].

UVA-transparent front encapsulant does not show fluorescence. This special situation of molecular transport (of UV absorber and oxygen within the encapsulant) results in the fluorescence square border in the UVF image (ring pattern).

Fig. 8 shows two different UVF patterns of fielded PV modules; one square pattern and a ring pattern UVF.

These two types of modules comprise of different encapsulants. The module with square pattern uses conventional UV-absorbing EVA (3M 9100), the module with the ring pattern uses UVA transparent EVA (3M 9110T) on the front side and UVA absorbing EVA (3M 9120B) on the rear side of the module.

Fig. 9 shows the UVF image of an outdoor aged PV module. The UVF above the solar cell is outshone by the fluorescence of the backsheet. In this case, the application of a logarithmic image scaling (Fig. 9 right) can reveal the cell crack pattern.

The UFV of a PV module comprised of UVA transparent EVA on front and rear side is very weak. Therefore, the exposure time required for taking a picture is one order of magnitude higher compared with modules with UVA absorbing EVA.

I. Influence of Backsheet Type on UVF Pattern

As the UVF formed in the polymeric encapsulant upon ageing/weathering can be extinct in the presence of oxygen and irradiation, the oxygen permeation properties of the backsheet are crucial for the UVF patterns formed, see Fig. 2 [39].

If polymeric backsheets are used, oxygen permeating into the encapsulant via the breathable backsheet act to be a bleaching agent for fluorescence. The steady-state rate at which oxygen gas permeates through a film at specified conditions of temperature and relative humidity is called oxygen transmission rate (OTR) and provides a measure for the oxygen permeability. The OTR (measured at 23 °C and 50% r.H. according to ASTM F 1927:2005) for polymeric backsheets can vary quite drastically from 4.5 $cm^3/(m^2$ d bar) for typical polyester (PET)-based backsheets, to 100 $cm^3/(m^2$ d bar) for polyamid (PA)-based backsheets and to 275 $cm^3/(m^2$ d bar) for PO-based backsheets [40]. Consequently, the broadness of the rim around the cells of extinct fluorescence is strongly dependent on the OTR of the backsheet (see Fig. 10).

Barrier materials like glass or Al-foil containing polymeric backsheet laminates block the oxygen transport and water vapor ingress into the module stack (except for the edges of the module). Thus, provided a uniform encapsulation composition, the fluorescence formed within the encapsulant upon irradiation is uniform across the whole module area.

Fig. 11 shows an example of a PV module using a nonbreathable backsheet with an integrated metal foil. Different grades of EVA were used for the encapsulation: UVA transparent for the front and UVA absorbent for the rear. As mainly, the additives of the rear EVA show fluorophoric groups, enhanced UVF is

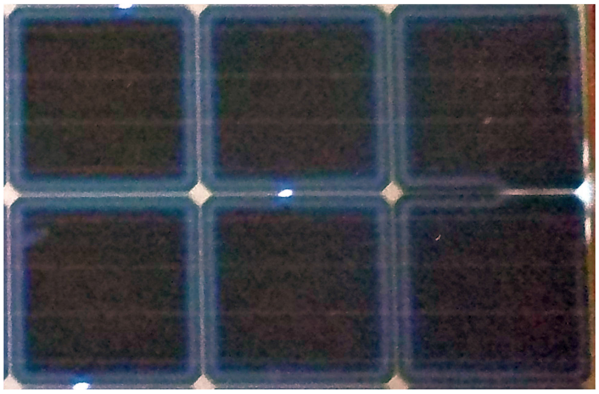

Fig. 11. Zoomed UVF image of PV module using a backsheet with metal foil and a cell with a crack in the lower left corner.

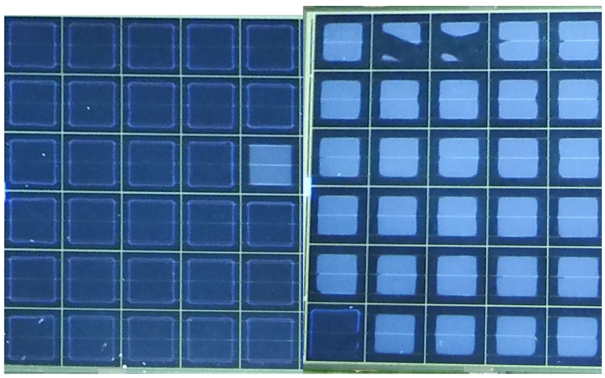

(a) (b)

Fig. 12. UVF image (a) of a ring pattern module with one repaired square pattern cell. UVF image (b) of a square pattern module with one repaired ring pattern cell.

detected along the gaps between cells and the cell edges as well as above cell cracks (Fig. 11). In this case, the cell crack appears brighter than the other areas of the front encapsulant, because the UVA absorber of the rear EVA diffuses to the front side through the crack. The UVA absorber initiates in combination with UV radiation the generation of fluorescent groups. The photobleaching process along the crack and the cell gaps cannot take place because of the missing oxygen. It is noteworthy that if the same type of EVA is used for the front and rear side, the cell cracks will not be visible in UVF image in the case of a nonpermeable rear side of the module. Most bifacial double glass modules use UVA transparent EVA on both the front and the rear side. For these PV modules, cell crack detection via UVF inspection is not applicable. The only double glass module design with the material combination UVA transparent EVA in the front and UVA absorbent EVA in the rear allows crack detection with UVF. These modules show a similar pattern like Fig. 11.

J. Repaired PV Modules

Fig. 12 shows examples for different UVF pattern types within one module. This can be the result of module rework in the production process. A defect cell was cut out together with the EVA and backsheet, and replaced by a new cell, EVA and backsheet and laminated again. As different EVA types were used in rework, different UVF pattern are visible in one module. The module shown in Fig. 12(a) comprises of UVA transparent EVA and rework using conventional EVA. In Fig. 12(b), an opposite case is shown.

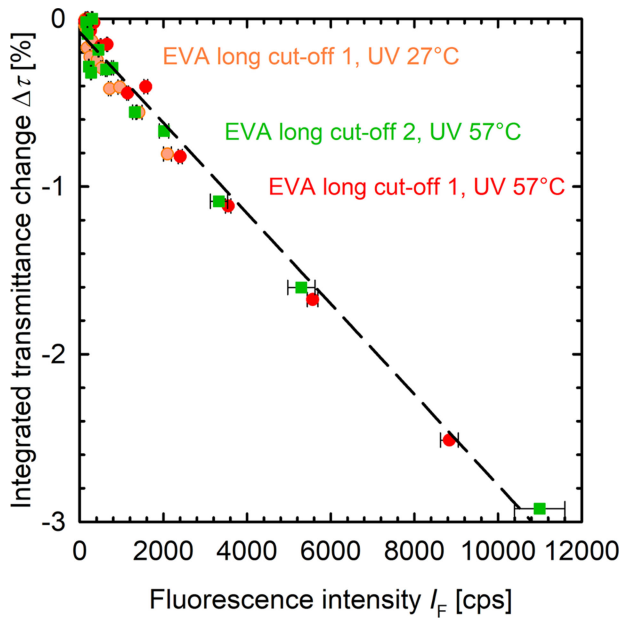

Fig. 13. Integrated transmission change to be a function of the UVF emission intensity of the UV exposed EVA samples at different temperatures [38].

K. Browning/Yellowing and UVF

As described already earlier, fluorophores are formed under UV exposure in the encapsulation (and sometimes backsheet) materials. The UVF intensity has been proven to be spatially correlated (in a quantitative way) with the integrated transmission loss in the visible spectral range [38].

The integrated transmission loss in the wavelength range 380 to 700 nm of three different EVA materials exposed to artificial UV doses of up to 890 kWh/m² at a temperature of 27 or 57 °C was measured. The EVA material showing a short cut off wavelength reveals no significant UVF increase or transmission decrease. Fig. 13 shows the loss in transmission to be a function of the UVF intensity of the samples for the long cut off EVAs and reveals a clear correlation between these two properties.

Optical simulations in the same work have shown that the resulting current density loss of an encapsulated solar cell is also linearly correlated to the UVF intensity.

L. Other Known Features

A one-of-a-kind observation is shown in Fig. 14. Seemingly, an adhesive tape that was forgotten on a module front glass absorbs UV light. This reduces the formation of fluorophores in the underlying EVA. Residues of said tape are removed during laboratory measurements.

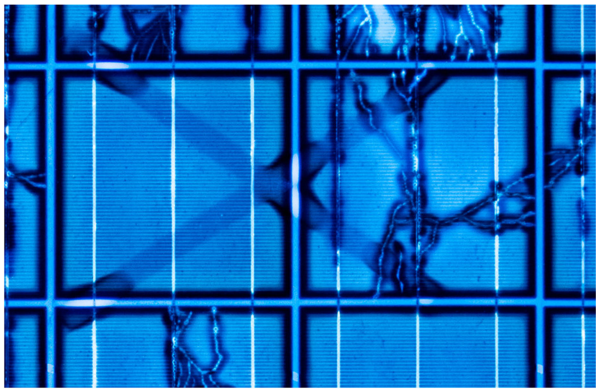

Fig. 14. UVF close-up of a PV modules in which the cells suffered from hail impacts. However, the more predominant effect is that two transparent adhesive tapes forming an "X" were found on top of the front glass.

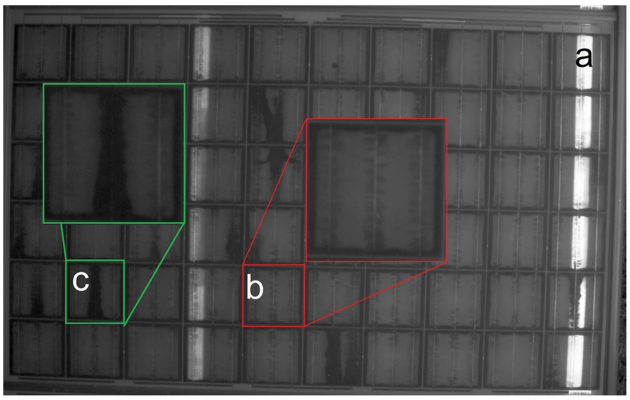

Fig. 15. (a) Bright stripe UVF pattern across the PV module can be found. Further specific features appear (b) along the cell finger metallization and (c) photobleaching along the bus bar. The modules are exposed for two years in south Germany.

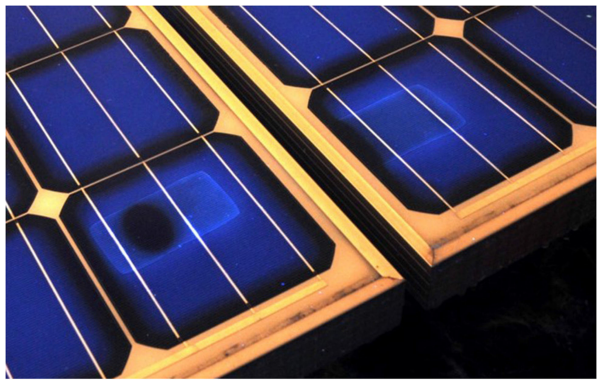

Fig. 16. UVF close up of PV module with a strange UVF feature.

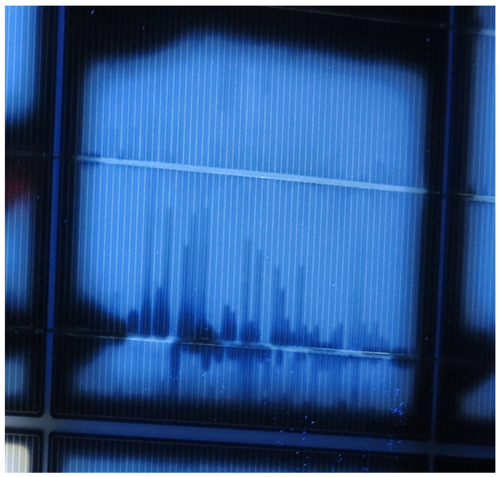

Fig. 17. UVF close up of PV module with finger-structure parallel annihilation.

In some modules, tapes fix the cell strings in between the strings before the lamination process. These tapes will stay in the laminate. These fixing tapes cause a typical pattern in the UVF images by changing the diffusion path in the module or by fluorescing themselves. The pattern of string fixing tapes can be seen, e.g., in Figs. 5 and 19.

Furthermore, some modules show fluorescence strips parallel to the short side of the PV module as shown in Fig. 15(a). These fluorescence stripes originate from the beginning of an original packed 100 m EVA roll. The manufacturer recommends not to use this first EVA film in the length of the roll circumference of the EVA roll in production. A comparable effect was observed within two PV modules as shown in Fig. 16. The special UVF are, e.g., residue of a peeled off label either on the glass or the encapsulation material.

M. Not Yet Understood Features

In some cases, the UVF parallel to cell interconnect ribbons is photobleached in a PV module, as seen in Fig. 15(c). There are at least two possible reasons for this photobleaching effect. First, a cell crack below the cell interconnect ribbon could cause photobleaching. However, in this case, the cell crack cannot be identified in an EL image because the crack is hidden by the ribbon. Second, cell interconnect ribbons are often wider than the silver bus bar on top of the solar cell. Therefore, the cell interconnect ribbon has not always a flush contact to the cell surface besides the bus bar. A rough textured cell surface, a high bus bar, a thin tin coating on the cell interconnect ribbon, and a too quick lamination process may provoke a gap between the ribbon and the cell surface next to the bus bar. Along this gap, there might occur an open channel starting from the cell edge leading oxygen and water vapor along the cell interconnect ribbon. This might promote photobleaching along the cell interconnect ribbon.

Another unexpected UVF feature that was observed in multiple independent cases is a decreased UVF along the fingers of the cell metallization as shown in Figs. 15(b) and 17. As the width of the darkening is limited to the fingers distance, and the length of the darkening varies with the individual finger, a physical interaction between a diffusion process and the fingers seems likely. Commonly, fingers are created using a printing process of a silver-particle-based paste. The paste is sintered to the cell in a firing process. These sintered particles may result in partly porous finger metallization [41]. The porosity has a

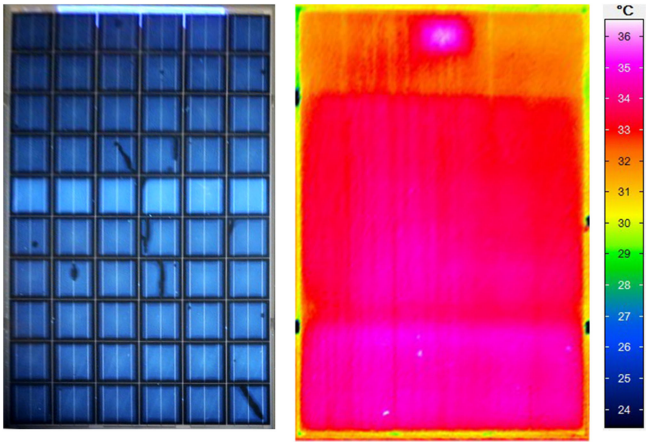

Fig. 18. Stripe-patterned UVF (left) that does not correspond to a heat up of the involved cells in thermography (right).

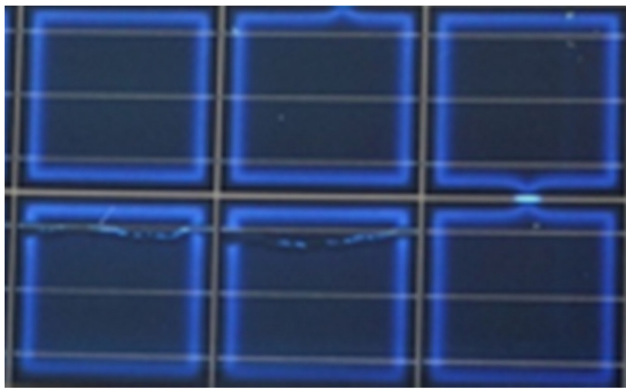

Fig. 19. Bright cracks in ring pattern image. The UVF pattern is photobleached where the crack crosses the ring pattern. On the right side a fixing tape can be seen between the cells.

potential to influence the diffusion speed of molecules along the bus bar and finger metallization. However, the authors are not aware of any detailed analyses at the time of writing.

In rare cases, it can be observed that the encapsulant shows an increased UVF along one cell row. While similar patterns could be caused by increased cell temperature (e.g., by MPP-current mismatch), no temperature rise was observed in this case, see Fig. 18. The origin of this effect is unclear.

Fig. 14 shows a fluorescent backsheet in the cell gaps. This proves that the fluorescent molecules from the backsheet are not photobleached. We suppose that depending on the age of the cell crack the fluorescent molecules of the backsheet diffuse through the cell cracks and form a fluorescent line directly above the cell crack. The UVF of the front lamination material is still photobleached along the cell crack.

The UVF image in Fig. 19 shows small bright fluorescent lines directly above cell cracks. Additionally, also photobleaching takes place along the cell cracks, because the UVF is interrupted where the crack crosses the ring pattern. Thus, the image shows probably a module with a backsheet open for oxygen diffusion. If UVA absorber would diffuse from the rear to the front, then the

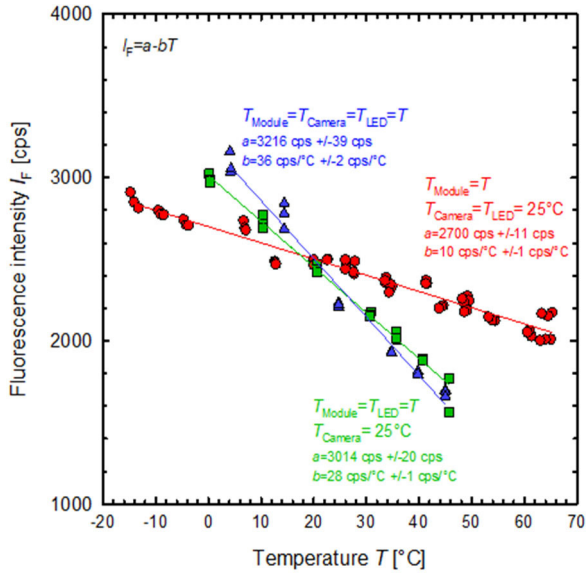

Fig. 20. UVF intensity of EVA over a cell in a PV module to be a function of the module temperature in different measurement cases. In red (dots), for a setup in which the camera and LED temperatures are stabilized, in green (squares), when only the camera is temperature stabilized. In blue (triangles), when all system components are at the same temperature as the module. The lines are linear fits; parameters are given with the respective datasets.

UVF pattern along the cracks should still have a photobleached line directly on top of the cell crack. But this is not the case. In the case of fluorescent molecule groups from the backsheet, the cell gaps should also fluorescence. However, it does not. This effect is not yet understood.

IV. Parameters Influencing UV Fluorescence

A. Temperature of the Module During Measurement

The fluorescence quantum yield of fluorophores is defined as the ratio between emitted photons and absorbed photons for a given substance. Considering that the absorption of a photon leads to an excited state, this fluorescence quantum yield depends on the competition between radiative and nonradiative deactivation. Both deactivation mechanisms have different activation energies and the quantum yield depends, therefore, on the temperature. The fluorescence quantum yield of aromatic compounds is known to decrease with increasing temperature [42].

To test the influence of the PV module temperature on the UVF intensity, a PV module was brought to the desired temperature in a climate chamber [43]. The module was briefly taken out to take an UVF image. The image setup consisted of the camera and the LED arrays, which were kept between 20 and 25 °C during the measurements.

Fig. 20 shows the UVF intensity measured over a cell of an aged, fluorescing module to be a function of the module temperature. The UVF intensity was measured once during the heating of the module from −15 to 65 °C and once again during cooling in the same temperature range. In this experimental setup, the UVF intensity shows no hysteresis to be a function

of the temperature depending on the cooling or heating of the module. Thus, we have shown that the temperature-induced changes in fluorescence intensity are reversible and that the temperature range and duration are small enough to prevent the formation of new fluorescence molecules. Therefore, we can conclude from Fig. 20 that the UVF intensity of the aged module decreases when the temperature of the PV module is increased.

B. Temperature of the UV LED Source During Measurement

The efficiency of LEDs decreases with increasing temperature. In addition, a shift of peak wavelength of up to 8 nm toward higher wavelengths by increasing the temperature from 20 to 120 °C has been observed for UV LEDs [44]. If the LED temperature is increased independently from the module temperature, the fluorescence emission intensity of the module decreases. The temperature of LEDs increases during their operation. For this reason, the UVF intensity may not be linearly correlated to exposure time when the extended exposure time leads to relevant heating of the LED. The effect of the environment temperature on UV light intensity emitted by the LED is depending on the cooling system of the LED arrays. To show the influence of the LED temperature on the fluorescence measurement, we measured the UVF intensity of the same area of the same module as in Section IV-A. The measurement is done in a climate chamber at temperatures ranging from 0 to 45 °C. In this configuration, the module and the LEDs are at the chamber temperature, while the camera is maintained at constant temperature in an insulated box. In Fig. 20, the UVF intensity is shown to be a function of the chamber temperature. In this case, the temperature coefficient of the UVF intensity is almost three times higher than the fluorescence temperature coefficient of the module alone.

C. Temperature of the Camera During Measurement

Charge coupled device arrays are—like LEDs—subject to temperature effects. An increasing temperature increases the dark field current of each pixel bin and therefore reduces the sensitivity range of the camera. To assess the extent of the influence of the camera temperature on the UVF intensity, we used the same setup as in Section IV-B without insulating the camera. The UVF intensity measured in this configuration is shown to be a function of the temperature in Fig. 20.

The temperature dependence of the UVF intensity in this configuration is slightly higher than when the temperature of the camera is stabilized. Nevertheless from the comparison of three curves, it is obvious that the temperature of the LED arrays is a critical factor, followed by the module temperature. For this reason, it is recommended to measure UVF intensity in the field under moderate temperatures, in the range from 0 to 20 °C. Furthermore, an adequate LED cooling system should be integrated in the system during its conception.

D. Temperature History of PV Module

The PV module temperature plays a considerable role in the kinetics of fluorophores formation. Under the same irradiance level and exposure time, the UVF intensity increases faster in a sample held at 57 °C than in an equal sample at 27 °C [10]. Under natural conditions, temperature effects are also observed. Fig. 21 shows the infrared (IR) image of a short-circuited PV module taken under ca. 800 W/m² at an ambient temperature of 28 °C during a summer day. The module temperature was measured on the backsheet surface behind each cell.

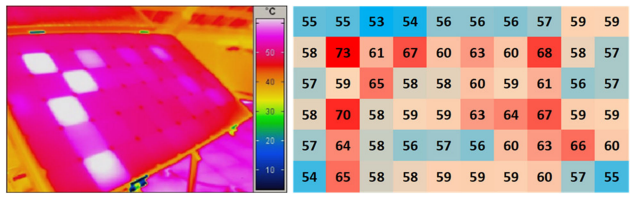

Fig. 21. Infrared image (left) and backsheet temperature map in °C (right) of a short-circuited PV module under 800 W/m² sun exposure and 28 °C AT.

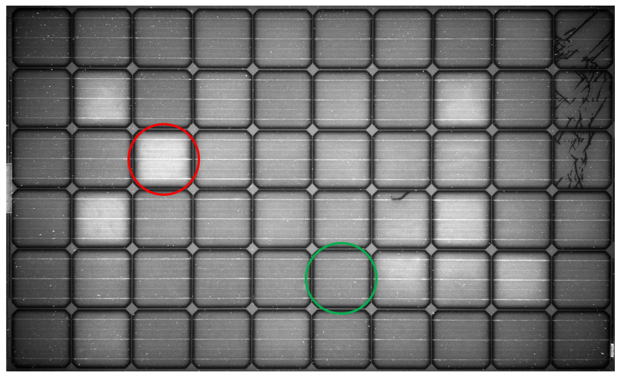

Fig. 22. UVF image of a PV module with cells operating at different temperatures. The red and green circles mark cells that operate at 65 and 56 °C, respectively. Conditions: under 800 W/m² irradiance and 28 °C AT.

Fig. 22 shows the UV-F image of same module after 77 days of outdoor exposure taken in the lab at 25 °C without natural light. The module has been allowed to cool down to room temperature before the image has been taken. The UVF intensity on each cell is almost homogeneous, although there is a significant discrepancy in UVF intensity from cell to cell. By comparing this UVF image with the obtained cell temperature pattern of the IR picture or the temperature distribution on the backsheet, a strong correlation between the temperature under sun exposure and the UVF intensity in the dark is noticeable. This shows that the UVF imaging highlights the hotter parts of the module and that the fluorophores retain the information even after the module has been disconnected and dismounted. Thus, the UVF imaging allows the detection of present or past heat-producing issues in the module without requiring the module being contacted.

Fig. 23 shows the UVF intensity measured over two selected cells to be a function of the global irradiation. The initial fluorescence originates from the manufacturing process as described in Section III-B and is fully photobleached after 10 kWh/m² of UV dose. We speculate that the rapid initial photobleaching takes place by consuming the oxygen content incorporated during the production process.

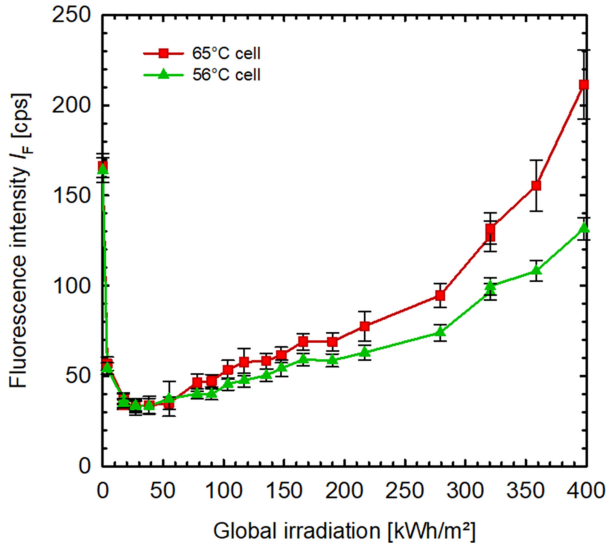

Fig. 23. UVF intensity to be a function of the irradiation dose measured over two cells with different operating temperatures. The lines are a guide to the eyes. The red squared and green triangle measuring points correspond to the red and green marked cells in Fig. 22.

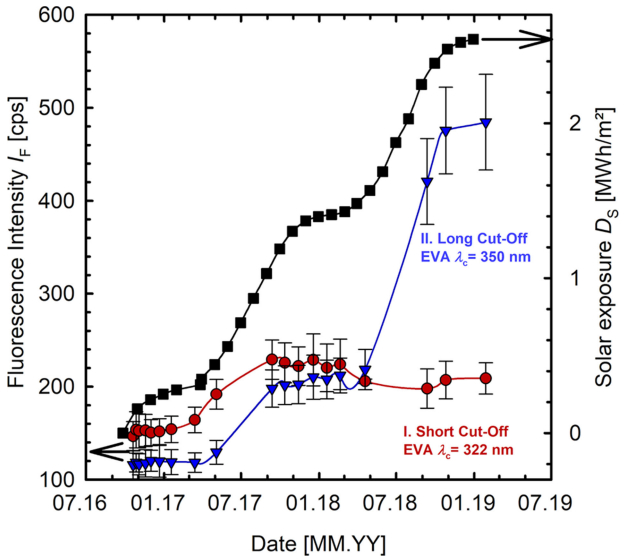

Fig. 24. UVF intensity measured zones to be a function of time on modules with encapsulation materials having cut off wavelengths of 322 nm (red dot curve) and 350 nm (blue triangle curve) exposed in Hamelin, Germany. The black square curve shows the accumulated sunlight dose since the installation.

Both cells are exposed to the same dose and irradiance but their operating temperature at 800 W/m² irradiance differs by 9 °C. The temperature difference leads to a significant difference in the fluorescence emission of both cells already after an exposure dose of 150 kWh/m², which in this case, corresponds to three weeks in summer.

E. UV Dose of PV Module

Fig. 24 shows the seasonal change of the UVF intensity increase as measured on two 9-cell modules exposed on a roof

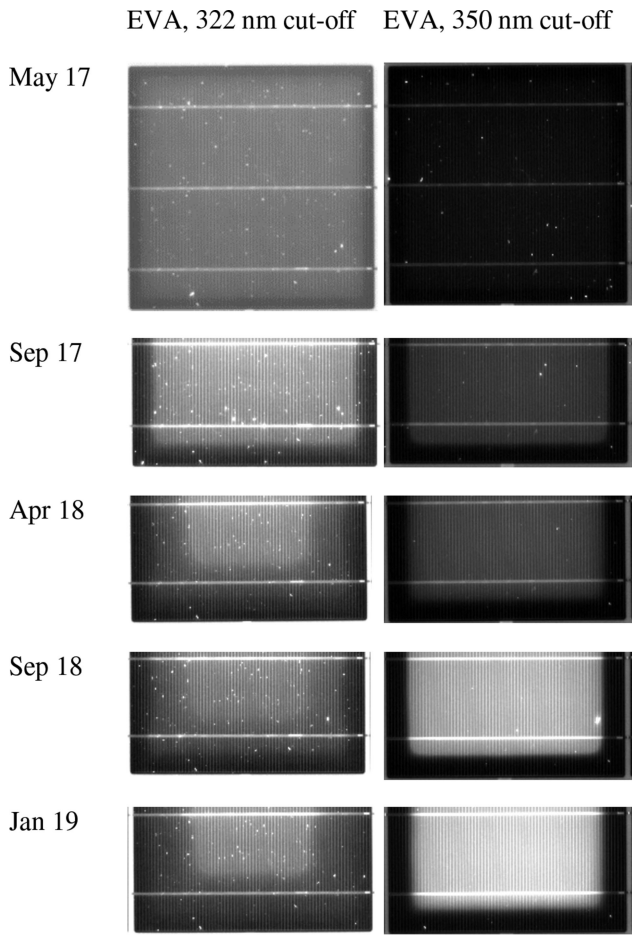

Fig. 25. UVF image of a cell (half) of two outdoor exposed modules with different EVA cut off wavelength. Images were taken at different times in Hamelin, Germany, over two years.

in Hamelin, Germany [10]. One of the modules contains an EVA encapsulant with a cut off wavelength of 322 nm, the other with 350 nm. Both modules are laminated with the same backsheet. The UVF intensity increases for both materials during the first summer and then stabilizes in the case of the short cut off EVA. A slight decrease of the UVF intensity is observed during the winter. The EVA with the 350 nm cut off wavelength shows an increase in both summers, the second one being higher than the first one, although the irradiation dose in the second summer was not significantly higher than in the first summer. This is consistent with the observation that for samples exposed to artificial UV continuously, the UVF intensity increased in a quadratic function of the dose D at constant temperature and irradiance [38]. This observation supports the statement that the increase of absorbance in the UVA spectrum accelerates the generation of fluorophores. For both EVA types, only one month in the field during summer time is sufficient to observe detectable UVF. In the winter, no relevant amount of fluorophores are generated.

Besides the seasonal variation of the UVF intensity increase over the middle of the cell, a seasonal variation of the photobleaching extent for both EVAs was observed. Fig. 25 shows

UVF images of the central cell of both modules at different dates. Over the first summer of exposure, both types of EVA develop a typical square UVF pattern with the usual extinction frame at the edge of the cell. During the first fall and winter, the EVA with the 322-nm cut off wavelength shows a decrease of the UVF intensity over a broader frame along the cell edges. In April 2018, three concentric square UVF intensity zones appear, as the cell edges remain darker than the intermediate new ring zone. In the second summer, the UVF intensity over the intermediate ring increases again, while the intensity over the central zone decreases. In the second winter, the area of the most intensively fluorescing zone is reduced and the frame area and ring area have fusioned. For the EVA with the 350-nm cut off wavelength, the edges of the frame that appeared after the first summer lose contrast and the fluorescing area slightly decreases. In the second summer, the UVF intensity increases drastically but the fluorescing area does not extend. Over the second winter, the frontier between the frame and the central area is once again losing contrast.

The observation made for both materials suggest that the competition between the mechanisms of formation of fluorophores and their photobleaching in the presence of oxygen is depending on the solar irradiation and temperature.

F. Photobleaching Rate of UV Fluorescence

When a new cell crack appears in an already fluorescing glass/backsheet PV module, the photobleaching mechanism depicted in Fig. 2 takes place. The UVF intensity starts to decrease along the crack, provided that the module is still exposed to sunlight. Fig. 26 shows the UVF intensity measured across a cell crack newly formed in an already fluorescing module. At the same time, the UVF profile is measured across an older crack. The fluorescence profiles depicted are measured after subsequent sun exposure after the formation of a new crack in summer. The fluorescence profile across the older crack remains unchanged during the whole measurement campaign. The UVF intensity over the new crack is decreasing. But even after three months, the UVF intensity is higher over the new crack than over the older crack. This makes it possible to read the temporal sequence of the cell cracks from their UVF image.

Authors have shown that UVF images of a PV module with UVA absorbing EVA can reveal transportation-induced cracks in a new PV module as soon as 11 days after installation in summer, with an equivalent sunlight dose of 55 kWh/m² [10].

G. Humidity Dose

Upon storage of PV modules with permeable backsheets in the climate chamber at high humidity and temperature fluorescence builds up in the polymeric encapsulant. This is typically the case for damp heat (DH85) tests according to test MQT 13 in the IEC 61215-2 Standard [45]. These fluorescent effects are related to the ingress of water vapor into the polymeric encapsulant and are not homogeneously distributed over the whole module. The fluorescing effects are stronger above the backsheet and the edges of the cells. The broadness of the fluorescent edges increases with increasing storage time and is related to water vapor permeation into the encapsulant via the polymeric backsheet [14]. The observed UVF patterns after DH storage (see Fig. 27) are clearly different from those observed after outdoor weathering or artificial irradiation of PV module.

Increasing the stress load to 90 °C and 90% r.H. (DH90) gives an even more distinct pattern of strong UVF between the cells and over the edges of the solar cells while keeping an

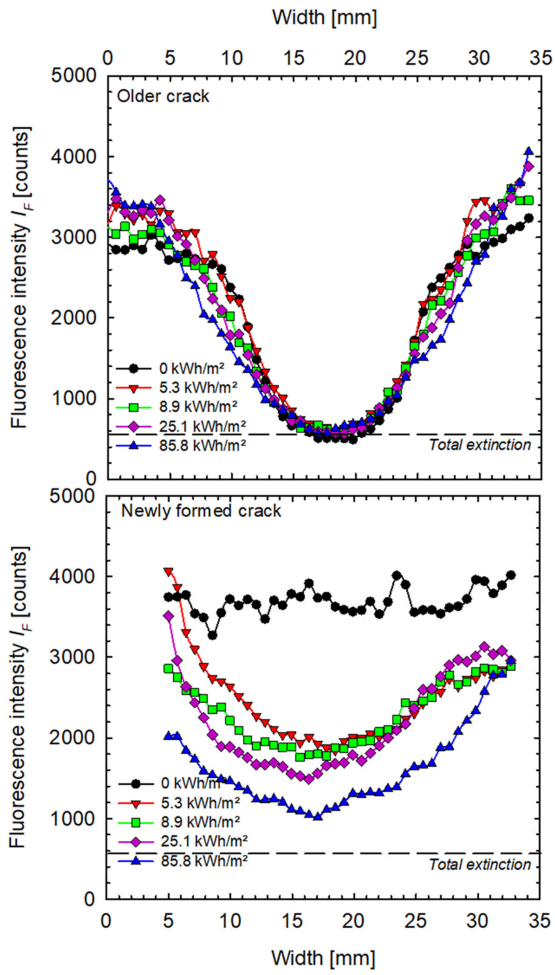

Fig. 26. UVF intensity profiles measured after sequential sun exposure across two cracks in a PV module: Top: perpendicular to an old crack, and bottom: perpendicular to a crack newly formed at 0 kWh/m². The dashed line represents the UVF level of areas that have been exposed to oxygen for several years such as cell edges.

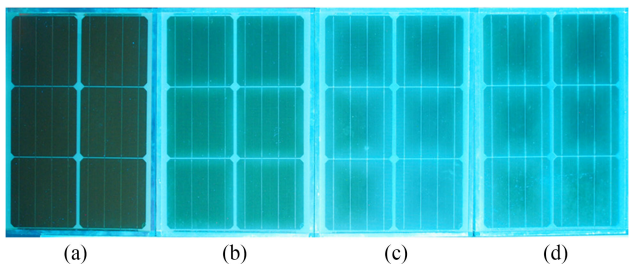

Fig. 27. Evolution of the UVF effects with increasing ageing time (a) original state, (b) 1000 h, (c) 2000 h, and (d) 3000 h at DH85 for a PV module with EVA encapsulant and permeable PET-based backsheet [14].

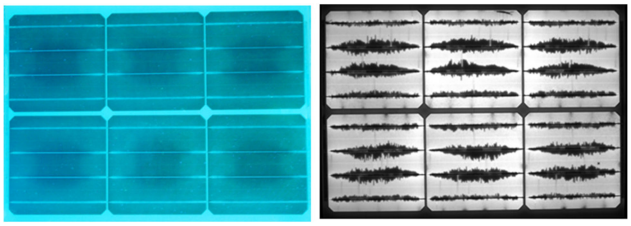

Fig. 28. UVF image (left) and EL image (right) of a 6-cell module with EVA encapsulant and permeable PET-based backsheet after 3000 h at DH90 [14].

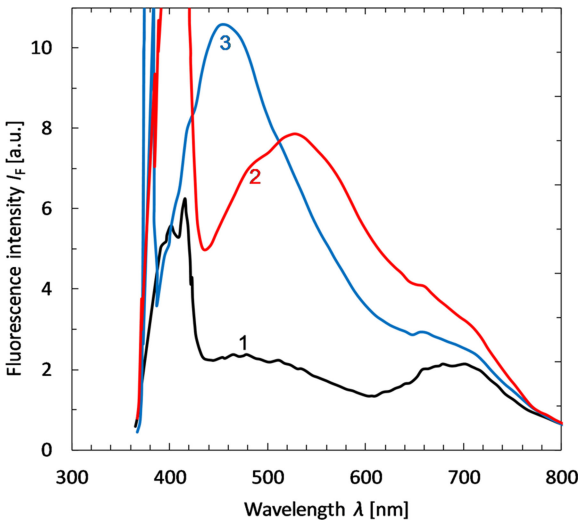

Fig. 29. UVF spectra from (1) cell center of an initial laminated module, (2) cell center of a UV aged module for 180 kWh, (3) from cell edge of a damp heat 85/85 aged PV module for 2600 h. Figure redrawn from [21].

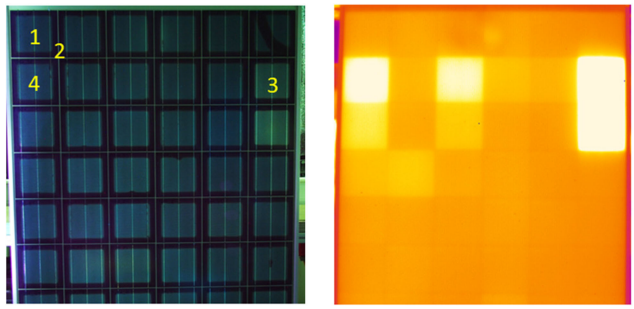

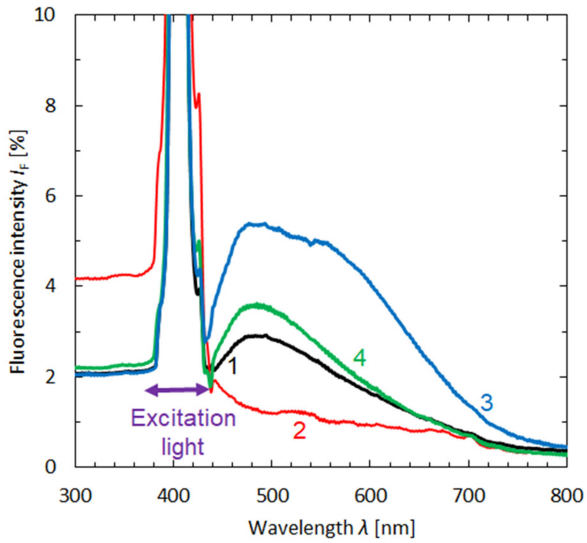

Fig. 30. UVF image (top left) with 400 nm excitation light, thermographic image in short-circuit conditions under illumination (top right), and UVF spectra (bottom) of the encapsulation of a naturally aged module measured at four different positions: (1) middle of intact cell, (2) between two cells, (3) middle of hot cell, (4) middle of moderate hot cell.

area with less UVF over the center of the cells. By comparing the UVF with the EL images of a test module stored at DH90 for 3000 h, see Fig. 28, it is obvious that corrosion effects of the silver finger along the bus bars are mainly focused in the center of the cells (dark areas in the EL image). In addition, performed thermo-desorption measurements with detection of the thermally desorbed substances by gas chromatography/mass spectrometry revealed the presence of free acetic acid in the encapsulant above the dark areas. There seems to be a correlation between the corrosion of the silver finger grid and the UVF pattern. However, the acetic acid corrosion cannot be identified by UVF.

H. Heat, Humidity, and UV Dose Influence the Spectrum of UVF

UVF-spectroscopic measurements of artificially or naturally aged PV modules show specific shifts of the UVF light in the front encapsulant, which depend upon the type of exposure (e.g., temperature, humidity, and irradiation). This spectral shift in dependence of the stress applied and the position within the module (center of a cell, between cells, above bus bars) was thoroughly studied by the group of Röder and Schlothauer [7], [47], [48]. Fig. 29 shows the UVF spectrum of artificial DH85 and UV exposure. The DH85 aged PV module shows two broad overlapping peaks in the range from 400 to 600 nm with a maximum at 470 nm. The UV loaded PV module shows a broad fluorescence distributed between 400 and 800 nm.

An example of a naturally aged module showing several hot cells during operation is given in Fig. 30. The fluorescence spectra measured at different positions of the module show different shifts of the UV-excitation light (@400 nm). The shift to 480 nm corresponds to ageing/weathering under outdoor conditions for five years in Austria. The additional peak with a maximum ~550 nm is attributed to fluorescing groups formed upon increased temperature of hotter cells within the module.

Thermally heavily degraded, already brownish PV encapsulation material can even fluoresce in the near IR spectrum [46], [49]. Therefore, an excitation within the visible red spectrum results in near-IR fluorescence of EVA. However, the observed fluorescence in the IR spectrum is much less intense than the blue response for typical UV excitation.

V. Detectable Failure Types for PV Modules and Arrays

Since the bill of materials of a PV module often makes the interpretation of the UVF images difficult, the examples given

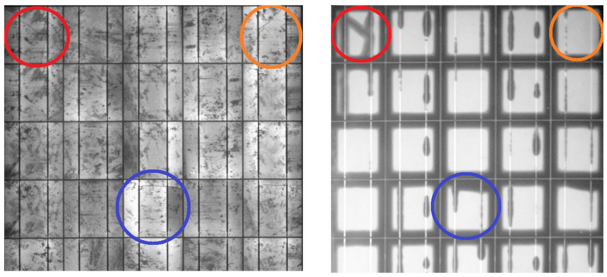

Fig. 31. Left image shows an EL image of a hailstorm exposed PV module. The right image shows the corresponding UV-F image with logarithmic scale. The blue circle marks an old cell crack. The red circle marks a cell crack that occurred during the hailstorm. The orange circle marks a cell crack, which occurred during demounting or transport to the lab after the hailstorm.

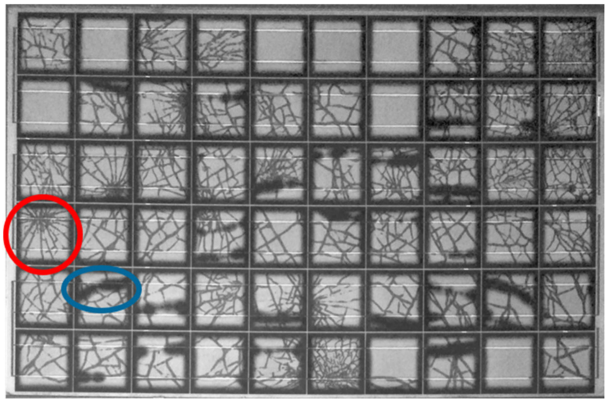

Fig. 32. Old (blue marked) and freshly formed (red marked) cell cracks in a logarithmic scaled UVF image.

in the following chapter are limited to those applications that allow unambiguous interpretation.

A. Cell Cracks

The main application of the UVF method most probably is the in-field detection of cell cracks in PV modules. However, one has to bear in mind that the photobleaching of the UVF along a freshly formed cell crack needs some summer days of exposure to take place and, consequently, make its detection via UVF possible. Therefore, the method cannot be applied before or directly after the installation of the PV modules. However, large PV systems are built in several months. Therefore, the UVF method should be applicable for cell crack detection after the complete installation of the system.

Freshly formed cell cracks in aged, sun exposed modules are up to 100 kWh of radiation dose distinguishable from older cracks. After higher radiation dose, new cracks may get indistinguishable to older cracks. Therefore, the method can be used to analyze the impact of a hailstorm on the cell crack pattern of PV modules [10], [11] several weeks after the hail event. Figs. 31 and 32 show PV modules exposed to a hailstorm. The PV module in Fig. 31 is hardly affected by the hailstorm, but allows a clear explanation of all phenomena that occur. An old cell crack appears broad and as dark as the UVF along the cell edge

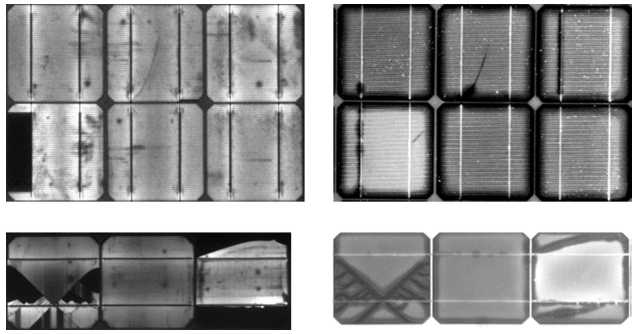

Fig. 33. Left: EL images of module parts with inactive cell areas [10]. Right: UVF images of the same module parts.

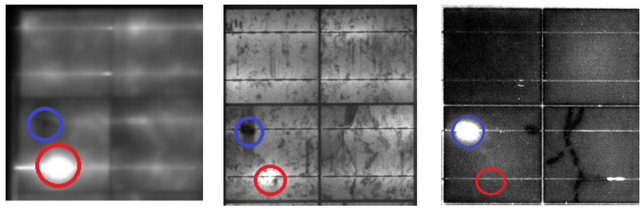

Fig. 34. Lock-in IR image (left) made at a current of 8.28 A; EL image (middle) made at a current of 8.23 A; UVF image (right). Old (blue circle) and new (red circle) hot spots are marked.

(blue mark). A freshly formed cell crack that was not exposed to the sunlight is not visible in the UVF image (orange mark). In this case, the crack occurs during demounting or transport of the module to the lab. The cell crack caused recently by a hailstorm is brighter in the UVF image than an old cell crack (red mark). To differentiate between new and old cell cracks, a logarithmic scaling is of the UVF image is useful.

B. Hot Spots

Hot spots can also be identified by UVF imaging. However, the UVF images have to be interpreted differently to IR-thermographic images. While an IR image shows the current temperature distribution in an operating PV module, the UVF image indicates the thermal history of each solar cell in the PV module. This allows for the detection of hot areas during operation of a PV modules during night or in the lab. Fig. 33 shows two examples of PV modules parts including cells with inactive cell areas. The inactive areas are so large that these cells block the current flow through the module, heat up during operation and consequently result in higher UVF intensity.

Other kinds of hot spots are also visible in UVF images. Fig. 34 compares the lock-in IR, EL, and UVF images of a part of a PV module showing problems with contact of the cell interconnect ribbons to the solar cell. One contact area has already burned out resulting in no electrical current flow (blue marked points). These points appear dark in the IR and EL images and are visible as burn marks on the backsheet (not shown here). In the UVF image, this burned out spots are still visible as highly fluorescent spots. On the contrary, the recently

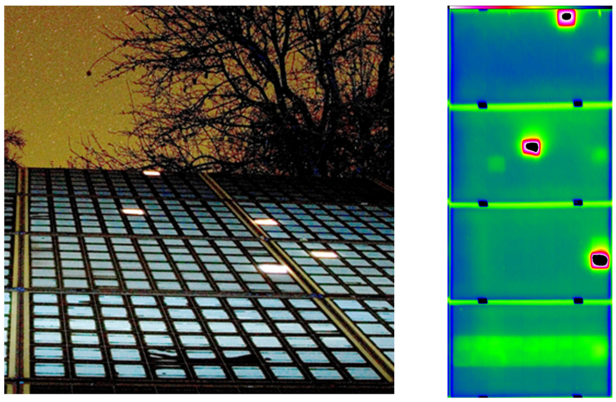

Fig. 35. Left: UVF image of PV modules showing hot cells (dark image regions are artificially brightened using image manipulation). Right: corresponding daylight IR image of the modules showing hot cells under working conditions.

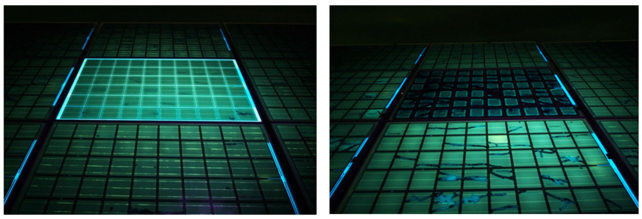

Fig. 36. UVF images of PV modules with identical service life and stress impact but varying bill of materials.

formed hot spot (red marked points) is rarely visible in the UVF image.

C. Hot Cells

In some cases, whole cells without visible cracks show fluorescence with much higher intensity than others, see Fig. 35. These cells most probably show a current mismatch to the other cells in the module and heat up.

D. Bill of Materials Differentiation

Different module designs in respect to varying types and/or qualities of encapsulants and backsheets cause varying fluorescence effects induced by 1) their permeation properties (mainly OTR), 2) chemical composition including additives (and their degradation products), 3) impurities, and 4) ageing induced reaction or decomposition products. UVF images taken in the field from the same installation site meaning identical stress factors as well as identical exposure time can reveal unequivocally if all module exhibit the same bill of materials or not. The example given in Fig. 36 shows UVF images that prove that different types of backsheets (PA, PET-based, PET+Al, Tedlar) result in different extinction patterns of the UVF [50]. Besides, also different EVA types with varying formulation result in clearly specifiable fluorescence behavior. The resulting UVF spectra clearly show a distinguishable shape, which can mainly be explained by differences in the additive mix of the EVA films used.

Especially for large PV systems, the compliance of the BOM of the PV modules with the data sheet is part of the sales contract. UVF imaging allows for fast and nondestructive detection of different BOMs installed. The identification of different BOMs is also useful for the choice of sets of modules to be analyzed, because different BOMs may show up different degradation modes.

VI. Measuring in the Field

A. Manual Setup

The UV light source for the excitation of the UVF should be easily portable, preferably lightweight and battery-powered. It should offer a high intensity of UVA, almost no visible blue light (>400 nm) and a high radiant flux at low electrical power requirements. Low cost UV LED torchlights often emit a higher portion of blue light (>400 nm), which may require additional filtering. In the end, the light has a lower UV conversion efficiency, which may require additional cooling and reduces battery life.

A simple UVA torch is useful for strategic sampling of test candidates for the more elaborate EL imaging. The overall presence and qualitative distribution of cell cracks is easily visible with the bare eye. Commercially available UVA torches with a single high efficiency UV LED typically emit a beam angle of 20° and offer a UV irradiance of about 3 W/m² at a distance of 1 m. This torch type allows for a sufficient UVF signal also suitable for close up photography of single cells with a standard digital camera or with a smartphone. The use of a tripod is recommended for good image sharpness. The required darkness is achieved at irradiation below 0.1 W/m² light intensity. This condition is typically achieved one to 2 h after sunset. Moon light or urban street light often poses only small imaging limitations.

As all imaging techniques for the inspection of PV modules preferably require a fairly perpendicular view onto the object of interest, the position of the UV source and the camera highly depends on the inclination angle and the general layout of a PV array. Because of the comparably low intensity of the UVF emission, long exposure times and a wide open aperture is necessary, which leads to a narrow depth of field. This means that with a flat viewing angle, only a limited area of the module has sharp image characteristics.

In utility-scale systems (PV parks), the rows of mounting tables incorporating several rows of modules normally allow for close access and viewing distances of at most a few meters. For the PV modules above the first row, a flatter viewing angle must be accepted or a specialized high rise camera stand can be used. In any case, a more distant setup from the object of interest is needed. Thus, the UV irradiance is considerably lowered and the UVF appears less distinct.

A camera with a remote shooting option from a tablet or laptop computer is favorable for easier focusing and picture control. The whole set of equipment should fit into a suitable case rugged enough for transport on a plane.

With good accessibility to the modules and suitable ground and weather conditions, about 250 modules per hour can be

processed on site, assuming one module per image allowing for the highest possible resolution of the seen features.

B. Day Time Setup

Recently, a measurement setup consisting of a hood in which UV LED arrays and a camera are integrated has been built to allow for day time measurements [10]. The hood is designed to be laid on the module to be examined with the size of the hood adjustable to the size of the PV modules. The length and width are adjustable from 98 to 115 cm and 165 to 175 cm, respectively, with 1 cm increments. The hood weighs around 8.5 kg for a typical 60 cell module size. The operator triggers and controls the capture by means of a smartphone connected through WLAN with a cube computer mounted on the hood. The UV LEDs deliver a power in the range of 3 to 5 W/m² at the surface of the module. The camera employed has a resolution of 24 Mpixel and ISO 1600. Typical exposure times are between 1 and 3 s. The whole system is powered by a 10 Ah (128 Wh) Li iron phosphate battery.

The hood provides easy positioning of the system including the positioning of the camera in the center of the module with a perpendicular view axis to the surface of the module. The hood stays stable during the whole exposure time.

The light coming from the rear side of the modules through the cell gaps can be eliminated by a dark field correction, meaning a picture without UV illumination is subtracted from the UVF image.

With a 1 or 2 s exposure time, up to 200 modules per hour can be captured by a single person under daylight.

C. Drone-Based Setup

In order to make the UVF inspection with drone easy and affordable, the requirements for selecting the drone are 1) a commercialized, inexpensive drone, 2) low skill demand for the pilot, 3) stable enough to take images in the dark with exposure time of about 0.1 s, 4) needs to carry a low noise camera and an additional UV lamp.

With the above considerations, a commercially available drone with a weight of 2935 g, max ascent speed of 5 m/s, max speed of 22 m/s, a max wind speed resistance of 10 m/s, and a max flight time of 18 min is chosen for the UVF inspections. The camera resolution is 9 Mpixel, ISO range 100–25 600 and exposure time 8∼1/8000 s. Two remote controls are used for the inspection. One is for the pilot to control the drone, and the other one is for the photographer to take pictures. Therefore, two persons are required for the inspection job.

Battery capacity is a major constraint for the drone inspection because the drone has to carry an additional UV lamp that seriously increases the weight of the whole setup. Furthermore, the battery also needs to supply power to the UV lamp which further reduces the flight duration. A battery package of 4.5 Ah allows a flight time of 8 to 10 min for still air conditions. For longer flying time, drone types with two batteries can be used to almost double the flying time.

Three 20-W UV LED chips are used as excitation light sources for the UVF lamp. An additional lens (to concentrate the cone of light to a beam angle of 51°), and a low pass filter are added on top of the LED chips. The UVF inspection with a drone is more limited than the IR inspection as the distance to the module surface strongly influences the detectable UVF signal intensity. The higher the drone flies, the weaker is the UV intensity at PV module level. As weaker intensities require longer exposure time for taking a picture. However, the drone is always moving and vibrating, the exposure time must be as short as possible. According to our experience, if the exposure time is above 0.1 s, the image becomes increasingly blurred.

In order to maintain the image quality, the drone is supposed to fly as low as possible. However, flying low increases the inspection time, consumes more power, and complicates the control of the drone. With the two contradictory height demands, we have to compromise to have acceptable image quality and inspection time.

Fig. 37 shows the UVF images taken at flight heights of 1.5, 4.5, 6, and 9 m with an integration time of 0.16 s. At 1.5 m height, the image is clear, but there is only one module in the image. The inspection time will be very long, and it is difficult to locate the defect module afterwards. At a height of 9 m, the UVF is too weak and the resolution is too low to identify defects. At the height between 4.5 and 6 m, 12 to 16 modules can be seen in one image, respectively.

In the case that the PV modules show “ring pattern” UVF with low intensity, the drone has to fly with low height to be able to catch one module in each image, the average time required is 4 s/module. The time for changing battery is not included, and it depends on the drone type and battery capacity. For PV modules showing “square pattern” UVF, the drone can fly at elevated heights of 4.5 m and take 12 modules in one image, the average time required is 0.5 s/module. Including the time for changing batteries, it is possible to inspect 720 modules per hour assuming battery exchange for six times. However, the inspection speed highly depends on the project design and weather conditions. The drone saves the inspectors from getting on the roof, and the test time is greatly reduced.

There are still some difficulties to perform the UVF inspection with a drone. First, the work has to be done in the dark, and flying in the dark increases the difficulty and risk of the drone damage. Second, most people are not willing to work at night, and it may increase the cost as well.

New module technologies applying UVA transparent EVA are detrimental to UVF inspection with drone. It makes UVF with drone much more time consuming. Therefore, manual or hood-based UVF inspection is recommended for this type of modules.

D. Occupational Safety

For good visibility and for photographic documentation of the fluorescent effects, a dark environment is favorable. As the human vision is not sensitive to light at wavelengths below 380 nm, the eye will not adapt to a brightness stimulus at lower wavelengths, i.e., the iris remains wide open in assumed darkness therefore the UV radiation can enter the eye and severely damage the fully exposed retina (photic retinopathy).

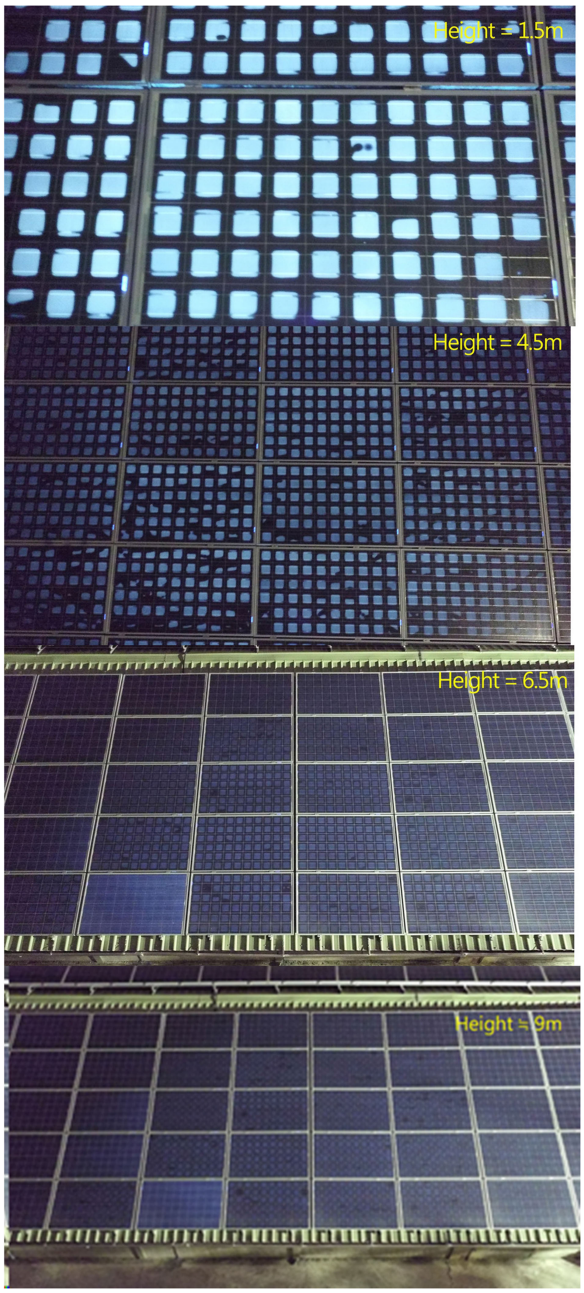

Fig. 37. UVF images taken at various flight heights.

Furthermore, painful sunburn-like effects can occur in the cornea and conjunctiva (photokeratitis) and on exposed areas of skin. It is therefore mandatory that protective measures for operating personnel as well as casual bystanders are implemented.

The safety standards for radiation exposure in most global regions are typically defined by ensuring the "state of the art." This is typically regarded to be the scientific publications of the "International Commission on nonionizing Radiation Protection" (ICNIRP). For UV radiation, the currently relevant document is "ICNIRP GUIDELINES on limits of exposure to ultraviolet radiation of wavelengths between 180 nm and 400 nm" [51]. It discriminates between the risks of exposure of the eyes, and the exposure of the skin. To evaluate the radiation safety of a UV lamp, it is necessary to measure the spectral intensity distribution of the emission at a distance where exposure might happen. This spectrum is convoluted with weighting function given in [51] that describe the relative harmfulness of individual spectral ranges. The convolution must stay below 30 J/m² for the skin and eye and the total not convoluted energy must not exceed 10^4 J/m² for the eye in order to preclude thermal effects.

For a hand-held UV torch, UV-400 protection goggles with uncolored glasses according to DIN EN 170 are recommended. Interestingly, wearing safety glasses in some cases also improved the visual contrast of the UVF observations. If the UV light cone of the lamp is close to the holding hand, it is advisable to wear UV protecting gloves. A hood-based UVF system must not be used with transparent UV protection glasses. However, the eyes and skin must be protected against sunlight by sun protection glasses, clothes, or sun milk if one works under sunny daylight conditions. To protect the eyes from direct UV exposure for drone setups, the inspectors must wear transparent UV protection glasses. However, the drone is most of the time quite a distance away from the inspectors therefore with our setup no protective measures have to be taken for the skin.

In any case, the UV irradiation exposure limits must be estimated for each individual setup. Access of unprotected persons to the examination area must be prevented to avoid unprotected eye exposure of uninvolved persons. As in all situations on site, two persons are necessary for safety reasons.

VII. Conclusion

The sometimes difficult evaluation of UVF patterns has been a drawback for its mainstream application for PV-plant inspections in recent years. Thus, the goal of this review is to clarify the interpretation of the UVF images as well as to describe how to apply the method in the field.

The UVF method enables to find cell cracks, hot cells/cell parts, or differentiate between different bills of materials in the polymer part of the PV modules. Cell cracks can be set into a chronological order of appearance with UVF. The UVF method is not able to identify potential induced degradation [52], light induced degradation [53], and acetic acid corrosion [54], [55] in PV modules. For the successful application of the UVF method, some conditions must be fulfilled. PV modules, which avoid oxygen diffusion, e.g., glass/glass or glass/aluminium backsheet modules, into the PV module allow only the identification of hot spots. PV modules without UVA absorbing agents show no or very little fluorescence. Under moderate climate conditions, the generation of fluorophores takes one month in the summer or three months in the annual transition periods to form sufficient fluorescent material for an analysis of new PV modules. In the winter, only very small changes in the UVF appear. Nevertheless, if these conditions are taken into account the UVF method is very simple to apply. No special weather conditions and no access to the module cables are needed. The method is applicable in daylight with a hood or at night with a handheld, tripod, or drone mounted UV source.

UVF adds in comparison to EL or IR thermography the ability to identify different module bill of materials in the polymer part of the PV modules and the chronological order of cell cracks. Together with IR thermography, the UVF images help to identify the elsewise missing cell cracks. But these methods need unequal environmental conditions. EL and UVF images may be taken in parallel in the field during inspection with little additional effort. For the EL method, additional UVF images allow to differentiate cell cracks in multicrystalline wafer from crystal defects and detect hotspot problems.

ACKNOWLEDGMENT

We thank M. Siebert for implementation of hood measurement technology and acquiring various images for this review.

REFERENCES

[1] B. N. G. Giepmans, S. R. Adams, M. H. Ellisman, and R. Y. Tsien, "The fluorescent toolbox for assessing protein location and function," *Science*, vol. 312, pp. 217–224, 2006.

[2] F. Leblond, S. C. Davis, P. A. Valdés, and B. W. Pogue, "Pre-clinical whole-body fluorescence imaging: Review of instruments, methods and applications," *J. Photochem. Photobiol. B, Biol.*, vol. 98, no. 1, pp. 77–94, 2010.

[3] D. Comelli *et al.*, "A portable UV-fluorescence multispectral imaging system for the analysis of painted surfaces," *Rev. Sci. Instrum.*, vol. 79, no. 8, 2008, Art. no. 086112.

[4] C. Carter-Snell and K. Soltys, "Forensic ultraviolet lights in clinical practice: Evidence for the evidence," *Can. J. Police Secur. Services*, vol. 3, no. 2, pp. 79–85, 2005.

[5] F. J. Pern, "Factors that affect the EVA encapsulant discoloration rate upon accelerated exposure," *Sol. Energy Mater. Sol. Cells*, vol. 41–42, pp. 587–615, 1996.

[6] D. L. King, M. A. Quintana, J. A. Kratochvil, D. E. Ellibee, and B. R. Hansen, "Photovoltaic module performance and durability following long-term field exposure," *Prog. Photovolt., Res. Appl.*, vol. 8, pp. 241–256, 2000.

[7] J. Schlothauer, S. Jungwirth, B. Röder, and M. Köhl, "Fluorescence imaging—A powerful tool for the investigation of polymer degradation in PV modules," *Photovolt. Int.*, vol. 10, pp. 149–154, 2010.

[8] J. Schlothauer, S. Jungwirth, M. Köhl, and B. Röder, "Degradation of the encapsulant polymer in outdoor weathered photovoltaic modules: Spatially resolved inspection of EVA ageing by fluorescence and correlation to electroluminescence," *Sol. Energy Mater. Sol. Cells*, vol. 102, pp. 75–85, 2012.

[9] M. Köntges, S. Kajari-Schröder, and I. Kunze, "Cell cracks measured by UV fluorescence in the fields," in *Proc. 27th Eur. Photovolt. Solar Energy Conf.*, 2012, pp. 3033–3040.

[10] A. Morlier, M. Siebert, I. Kunze, G. Mathiak, and M. Köntges, "Detecting photovoltaic module failures in the field during daytime with ultraviolet fluorescence module inspection," *IEEE J. Photovolt.*, vol. 7, no. 6, pp. 1710–1716, Nov. 2017.

[11] W. Mühleisen *et al.*, "Outdoor detection and visualization of hailstorm damages of photovoltaic plants," *Renewable Energy*, vol. 118, pp. 138–145, 2018.

[12] G. C. Eder *et al.*, "Non-destructive failure detection and visualization of artificially and naturally aged PV modules," *Energies*, vol. 11, no. 5, 2018, Art. no. 1053.

[13] W. Mühleisen *et al.*, "Scientific and economic comparison of outdoor characterisation methods for photovoltaic power plant," *Renewable Energy*, vol. 134, pp. 321–329, 2019.

[14] G. C. Eder *et al.*, "Climate specific accelerated ageing tests and evaluation of ageing induced electrical, physical and chemical changes," *Prog. Photovolt. Res. Appl.*, vol. 27, pp. 934–949, 2019.

[15] J. Schlothauer, C. Peter, C. Hirschl, G. Oreski, and B. Röder, "Non-destructive monitoring of ethylene vinyl acetate crosslinking in PV-modules by luminescence spectroscopy," *J. Polym. Res.*, vol. 24, no. 12, 2017, Art. no. 233.

[16] G. C. Eder, Y. Voronko, P. Grillberger, B. Kubicek, and K. Knöbl, "UV-fluorescence measurements as tool for the detection of degradation effects in PV-modules," in *Proc. Eur. Weathering Symp.*, Vienna, Austria, 2017, pp. 205–214.

[17] F. J. Pern, "Ethylene-vinyl acetate (EVA) encapsulants for photovoltaic modules: Degradation and discoloration mechanisms and formulation modifications for improved photostability," *Die Angewandte Makromolekulare Chemie*, vol. 252, pp. 195–216, 1997.

[18] F. J. Pern and S. H. Glick, "Fluorescence analysis as a diagnostic tool for polymer encapsulation processing and degradation," *AIP Conf. Proc.*, vol. 306, 1994, Art. no. 573.

[19] M. Köntges *et al.*, "Review of failures of PV modules," Report IEA-PVPS T13-01:2014, 2014, ISBN 978-3-906042-16-9.

[20] K. Grabmayer *et al.*, "Characterization of the aging behavior of polyethylene by photoluminescence spectroscopy," *Polym. Degradation Stability*, vol. 107, pp. 28–36, 2014.

[21] J. Schlothauer, "Evaluierung von EVA-Degradationsprozessen in Si-Photovoltaikmodulen mittels 2D-Lumineszenz," Ph.D. thesis, Humboldt Univ., Berlin, Germany, 2016.

[22] J. C. Schlothauer, K. Grabmayer, I. Hintersteiner, G. M. Wallner, and B. Röder, "Non-destructive 2D-luminescence detection of EVA in aged PV modules: Correlation to calorimetric properties, additive distribution and a clue to aging parameters," *Sol. Energy Mater. Sol. Cells*, vol. 159, pp. 307–317, 2017.

[23] Ch. Hirschl *et al.*, "Long term development of Photovoltaic module failures during accelerated ageing tests," in *Proc. 33rd Photovolt. Sol. Energy Conf.*, 2017, pp. 1709–1712.

[24] M. R. Vogt *et al.*, "Measurement of the optical constants of soda-lime glasses in dependence of iron content and modeling of iron-related power losses in crystalline Si solar cell modules," *IEEE J. Photovolt.*, vol. 6, no. 1, pp. 111–118, Jan. 2016.

[25] D. Ehrt *et al.*, "Redox equilibria and ultraviolet radiation induced defects in glasses," *Int. Congr. Glass*, vol. 1, pp. 84–93, 2001.

[26] J. S. Stroud, "Optical absorption and color caused by selected cations in high-density, lead silicate glass," *J. Amer. Ceram. Soc.*, vol. 54, pp. 401–406, 1971.

[27] D. E. King, F. J. Pern, J. R. Pitts, C. E. Bingham, and A. W. Czanderna, "Optical changes in cerium-containing glass as a result of accelerated exposure testing of PV modules," in *Proc. Conf. Rec. 26th IEEE Photovolt. Specialists*, 1997, pp. 1117–1120.

[28] A. Morlier, M. Köntges, S. Blankemeyer, and I. Kunze, "Contact-free determination of ethylene vinyl acetate crosslinking in PV modules with fluorescence emission," *Energy Procedia*, vol. 55, pp. 348–355, 2014.

[29] J. Schlothauer, R. Ralaiarisoa, A. Morlier, M. Köntges, and B. Röder, "Determination of the cross-linking degree of commercial ethylene-vinyl-acetate polymer by luminescence spectroscopy," *J. Polym. Res.*, vol. 21, no. 5, 2014, Art. no. 457.

[30] Y. Lyu, J. H. Kim, and X. Gu, "Fluorescence imaging on the cross-section of photovoltaic laminates aged under different UV intensities," in *Proc. IEEE 44th Photovolt. Specialist Conf.*, 2017, pp. 2844–2848.

[31] M. Köntges, S. Kajari-Schröder, and I. Kunze, "Crack statistic for wafer-based silicon solar cell modules in the field measured by UV fluorescence," *IEEE J. Photovolt.*, vol. 3, no. 1, pp. 95–101, Jan. 2013.

[32] I. Duerr, J. Bierbaum, J. Metzger, J. Richter, and D. Philipp, "Silver grid finger corrosion on snail track affected PV modules—Investigation on degradation products and mechanisms," *Energy Procedia*, vol. 98, pp. 74–85, 2016.

[33] P. Peng *et al.*, "Microscopy study of snail trail phenomenon on photovoltaic modules," *Adv. R S C*, vol. 2, pp. 11359–11365, 2012.

[34] S. Meyer *et al.*, "Silver nanoparticles cause snail trails in photovoltaic modules," *Sol. Energy Mater. Sol. Cells*, vol. 121, pp. 171–175, 2014.

[35] G. Pérez, D. Faye, B. Baradat, M. Ollé, and C. Noyes, "Detection and cleaning of flux residue inside connectors," in *Proc. 9th Int. Symp. Mater. Space Environ.*, 2003, pp. 521–526.

[36] G. T. Ayoub, "Flux inspection with UV fluorescence AOI," *Adv. Packag.*, vol. 13, no. 9, pp. 39–40, 2004.

[37] C. Peike, L. Purschke, K.-A. Weiss, M. Kohl, and M. Kempe, "Towards the origin of photochemical EVA discoloration," in *Proc. IEEE 39th Photovolt. Specialists Conf.*, 2013, pp. 1579–1584.

[38] A. Morlier, M. Siebert, I. Kunze, S. Blankemeyer, and M. Köntges, "Ultraviolet fluorescence of ethylene-vinyl acetate in photovoltaic modules as estimation tool for yellowing and power loss," in *Proc. IEEE 7th World Conf. Photovolt. Energy Convers.*, Kona, HI, USA, 2018, pp. 1597–1602.

[39] C. Peike *et al.*, "Impact of permeation properties and backsheet-encapsulant interactions on the reliability of PV modules," *ISRN Renewable Energy*, vol. 2012, pp. 1–5, 2012.

[40] Y. Voronko *et al.*, "Correlation of the loss in photovoltaic module performance with the ageing behaviour of the backsheets used," *Prog. Photovolt., Res. Appl.*, vol. 23, pp. 1501–1515, 2015.
[41] A. Ebong and N. Chen, "Metallization of crystalline silicon solar cells: A review," in *Proc. High Capacity Opt. Netw. Emerg./Enabling Technol.*, 2012, pp. 102–109.
[42] R. Kubin and A. Fletcher, "Fluorescence quantum yields of some rhodamine dyes," *J. Lumin.*, vol. 27, pp. 455–462, 1982.
[43] A. Morlier, M. Siebert, I. Kunze, S. Blankemeyer, and M. Köntges, "Influence of environmental conditions on UV fluorescence imaging in the field," in *Proc. IEEE 7th World Conf. P hotovolt. Energy Convers.*, Kona, HI, USA, 2018, pp. 1309–1312.
[44] Y. Xi *et al.*, "Junction temperature in ultraviolet light-emitting diodes," *Jpn. J. Appl. Phys.*, vol. 44, no. 10, pp. 7260–7266, 2005.
[45] *Terrestrial Photovoltaic (PV) Modules—Design Qualification and Type Approval—Part 2: Test Procedures 4.13 Damp Heat Test*, IEC 61215-2 Standard (version 1.0-2016.03).
[46] B. Röder, E. A. Ermilov, D. Philipp, and M. Köhl, "Observation of polymer degradation processes in photovoltaic modules via luminescence detection," in *Proc. SPIE Rel. Photovolt. Cells, Modules, Compon., Syst.*, vol. 7048, San Diego, California, USA, 2008, Paper 70480F-1.
[47] B. Röder, S. Jungwirth, M. Braune, D. Philipp, and M. Köhl, "The influence of different ageing factors on polymer degradation in photovoltaic modules investigated by luminescence detection," in *SPIE Proc.—Rel. Photovolt. Cells, Modules, Compon. Syst. III*, vol. 7773, Bellingham, WA, USA, 2010, Paper 7773-6.
[48] B. Röder, "Investigation of outdoor degradation of photovoltaic modules by luminescence and electroluminescence," in *Proc. SPIE Rel. Photovolt. Cells, Modules, Compon., Syst. III*, vol. 7773, San Diego, CA, USA, 2010, Paper 7773-19.
[49] B. Kubicek, R. Ebner, G. Újvári, H. Sonnleitner, and G. Eder, "Fluoreszenz-Effekte in der Photolumineszenz," Tagungsband von. Symp. Photovoltaische Solarenergie, Kloster Banz, Germany, pp. 112–113, 2015.
[50] S. Jungwirth, "The influence of different back sheet materials on EVA degradation in photovoltaic modules investigated by luminescence detection," in *Proc. SPIE Rel. Photovolt. Cells, Modules, Compon., Syst. III*, vol. 7773, San Diego, CA, USA, 2010, Paper 7773-11.
[51] International commission on non-ionizing radiation protection, "ICNIRP GUIDELINES on limits of exposure to ultraviolet radiation of wavelengths between 180 nm and 400 nm," *Health Phys.*, vol. 87, no. 2, pp. 171–186, 2004.
[52] W. Luo *et al.*, "Potential-induced degradation in photovoltaic modules: A critical review," *Energy Environ. Sci.*, vol. 10, no. 1, pp. 43–68, 2017.
[53] F. Kersten *et al.*, "System performance loss due to LeTID," *Energy Procedia*, vol. 124, pp. 540–546, 2017.
[54] U. Weber *et al.*, "Acetic acid production, mitigation and corrosion effects in ethylene-vinyl-actetate-(EVA) based PV modules," in *Proc. 27th Eur. Photovolt. Solar Energy Conf.*, 2012, pp. 2992–2995.
[55] T. Tanahashi, N. Sakamoto, H. Shibata, and A. Masuda, "Electrical detection of gap formation underneath finger electrodes on c-Si PV cells exposed to acetic acid vapor under hygrothermal conditions," in *Proc. IEEE 44th Photovolt. Specialist Conf.*, 2017, pp. 997–1004.